

Variation of Under-Etched Planes Appearing in Bulk-Micromachined Silicon Using TMAH Etchant

Les M. Landsberger, Mojtaba Kahrizi, Makarand Paranjape¹ and Sasan Naseh²

Department of Electrical and Computer Engineering, Concordia University
1455 deMaisonneuve Blvd. W., Montréal, Québec H3G 1M8, Canada

¹Instituto per la Ricerca Scientifica e Tecnologica, Trento, Italy 38100

²Department of Electrical Engineering, University of British Columbia, Vancouver, BC

(Received June 17, 1996; accepted September 13, 1996)

Key words: anisotropic etching of silicon, TMAH, underetch experiments, slow and fast etching planes, influence of IPA

Mask shapes and etch anisotropy of Si in a particular etchant determine the final forms of the etched structures. This paper considers the etching of $\langle 100 \rangle$ silicon in tetra-methyl ammonium hydroxide (TMAH) having a concentration between 25 wt% and 15 wt% at 80°C. Etch anisotropy, as seen in the under-etched inclined planes and in fast and slow etching planes, is found to be quite different in the two cases. In 25 wt% there is a deep local minimum in etch rate at the $\{100\}$ planes, while in 15 wt% there is a shallow local minimum at the $\{110\}$ planes. In between these two concentrations, more complex behavior is observed. The addition of isopropyl alcohol to the TMAH etchant further changes the etch anisotropy.

1. Introduction

Micromachining of structural features in bulk silicon relies on the fundamentals of anisotropic wet etching.^(1–11) This paper considers the etching of $\langle 100 \rangle$ silicon wafers, and focuses on a relatively new etchant, tetra-methyl ammonium hydroxide (TMAH). TMAH has received considerable attention recently^(12–19) because of its relative nontoxicity and compatibility with CMOS-based technologies.

Etch anisotropy is the variation of etch rate with direction in the crystal. In bulk silicon micromachining, the interaction of the etchant with the different Si lattice surfaces produces the anisotropic etch characteristic. Mask shapes and etch anisotropy of Si in a

particular etchant determine the final shapes of the 3-dimensional structures achieved. For example, convex vs. concave mask shapes yield completely different etched Si features. It is generally known^(1-11,20-22) that, because of geometrical considerations, etched concave shapes tend to expose the slowest etching planes, whereas etched convex shapes tend to expose the fastest etching planes. This phenomenon has been studied by many researchers and used advantageously, for example, in the etching of micropiercing structures.⁽²³⁾

The etching of an arbitrarily shaped concave mask pattern, such as that shown in Fig. 1(a), leads to the selection of slow under-etching planes. After a sufficient amount of etch time, only the slowest under-etching planes will remain.⁽¹⁾ These are the familiar $\{111\}$ planes. A convex shape such as that in Fig. 1(b), on the other hand, exposes fast etching planes, for example $\{411\}$ or $\{212\}$ planes. Note that the etched planes in the two cases differ both in their intersection with the top masked surface, and in their angle of inclination to the horizontal.

Etch anisotropy can vary substantially with etchant, etchant concentration, temperature and additives, leading to widely differing etched shapes,^(2,14,15,17-19,23-25) in both concave and convex structures. Specifically, Merlos *et al.*^(14,15) found that the addition of isopropyl alcohol (IPA) to TMAH changed the shapes of the resulting etched Si structures.

While full characterization of etch anisotropy would require etching of a 3-dimensional structure such as a sphere,⁽⁵⁾ this variation can be partially characterized by underetch experiments.⁽¹⁷⁻¹⁹⁾ Many researchers have employed underetch experiments as a practical method of obtaining information about etch anisotropy under particular conditions. Wagon-

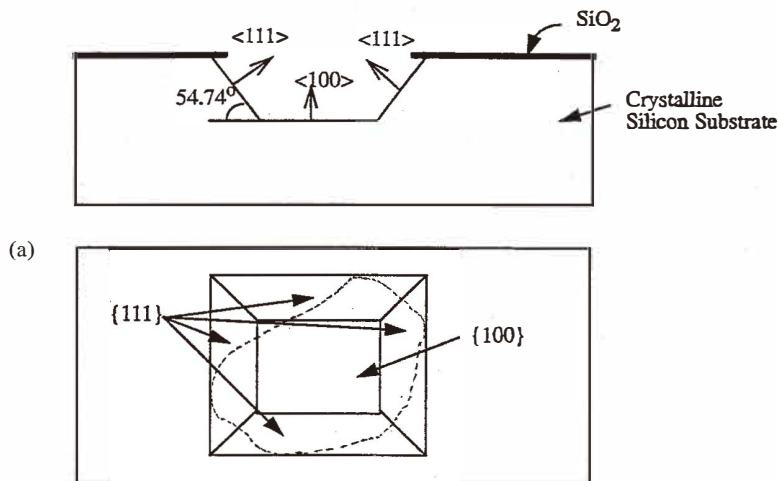


Fig. 1. (a) Cross-sectional and top view schematics of the etching of $\{100\}$ Si having an arbitrarily shaped concave mask opening. The dashed line indicates the edge of the opening in the masking oxide. The etch exposes slow etching planes, such that the final structure is bounded by a rectangle circumscribing the mask opening.

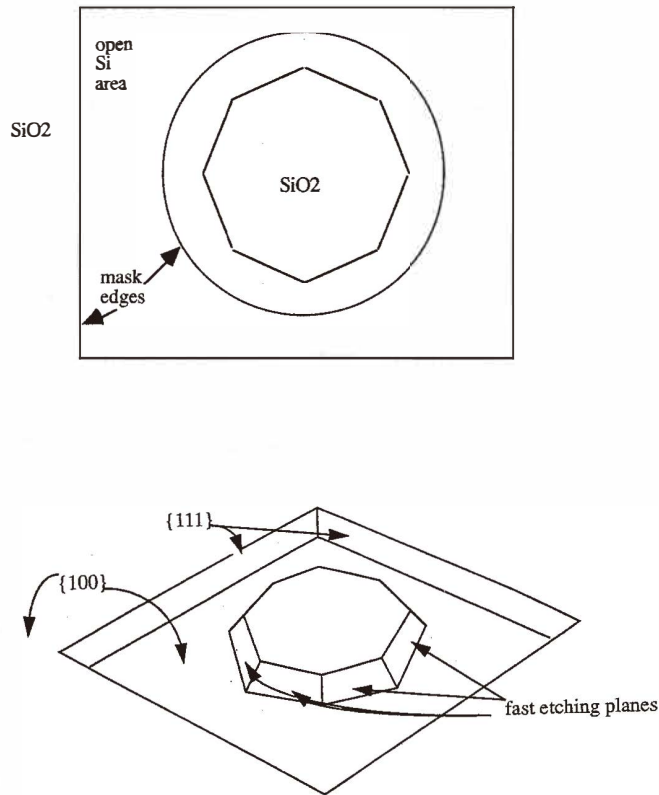


Fig. 1. (b) Top and perspective view schematics of the etching of $\{100\}$ Si having a circular convex mask shape inside a concave square. Fast etching planes are exposed by the convex features, while slow etching $\{111\}$ planes are exposed by the concave features. The masking oxide is not shown in the perspective view.

wheel patterns⁽²⁾ and triangle patterns⁽¹⁷⁻¹⁹⁾ have served to demonstrate differences between various etchant compositions.

This paper looks at the variation of etch anisotropy, and the slow and fast etching planes exposed, on masked $\langle 100 \rangle$ Si etched at 80°C in TMAH having a concentration between 25 wt% and 15 wt%. Experimental under-etch data is presented and discussed.

2. Etch Anisotropy in TMAH @ 80°C

Using a previously reported experimental procedure to characterize the etch anisotropy,⁽¹⁷⁻¹⁹⁾ n-type $\langle 100 \rangle$ Si wafers were oxidized and patterned. The mask pattern

consisted of sets of right-angled triangles, with two sides aligned in $\langle 110 \rangle$ directions (one of which was parallel to the wafer flat). The angle of the third side of each triangle was varied from 5° to 45° in intervals of 1° . In this way, $\{111\}$ planes were exposed on two sides of each triangle, and the variation of the under-etch rate with mask-edge deviation angle was studied by observing the behavior at the hypotenuse of each triangle.⁽¹⁷⁻¹⁹⁾ This set was mirrored and repeated until the full 360° was covered.

2.1. Under-etch rates

Figure 2(a) shows the under-etch rate of (100) silicon as a function of the mask-edge deviation angle, δ . In this figure, δ is measured from the intersection of a vertical (001) plane with the horizontal wafer surface. This intersection ($\delta = 0$) is at 45° from the $\langle 110 \rangle$ wafer flat. Because of the symmetry in the Si lattice, a plot of δ from 0° to 45° completely characterizes the under-etching of masked features on a $\langle 100 \rangle$ surface. However, a 90° span is shown here, so that the local minimum at $\delta = 0$ can be clearly seen. The under-etch rates for fresh, unstirred TMAH at 80°C , for 25 wt%, 21.2 wt% and 15 wt% are shown, as well that for 21.2 wt% with 15 vol% IPA. (The case of 21.2 wt% *without* IPA was prepared by diluting 25 wt% TMAH with DI water, while the case of 21.2 wt% *with* IPA was prepared by diluting 25 wt% TMAH with 15 vol% IPA. Note that 25 wt% was the maximum available concentration, and therefore 21.2 wt% was the maximum concentration that could be practically achieved after the addition of 15 vol% IPA.) All four curves have deep minima at $\delta = \pm 45^\circ$, corresponding to the slowest etching $\{111\}$ planes, and have maxima at about $\pm 15-25^\circ$ and local minima at $\delta = 0^\circ$.

2.2. Under-etched inclined planes

Figure 2(b) shows the graph of under-etched inclined planes for the cases described above. At $\delta = \pm 45^\circ$, the same $\{111\}$ planes (i.e. 35.3° to the vertical) are exposed in all cases, while the sets of results are strikingly different for each case at other deviation angles. In 25 wt%, the exposed planes vary monotonically from the $\{111\}$ to the *vertical* $\{100\}$, while in 15 wt%, the exposed planes vary monotonically from the $\{111\}$ to the *45°-tilted* $\{110\}$. In 21.2 wt% with IPA, the exposed planes are at almost exactly the same angles as those found at 15 wt%.

2.3. Derived etch rates

While Fig. 2(a) shows maxima and minima in *under-etch* rates, actual etch rates of the inclined planes can be derived from Figs. 2(a) and (b) using the formula:

$$(\text{etch rate of under-etched plane}) = (\text{under-etch rate}) \times \cos(\text{inclination angle})$$

These calculated inclined plane etch rates are plotted in Fig. 2(c) for the cases of 25 wt%, 15 wt% and 21.2 wt% with IPA. By inspecting the local maxima and minima in Fig. 2(c), and using the inclination angles at those extrema, fast etching and slow etching directions are found. Table 1 summarizes the differences between the cases.

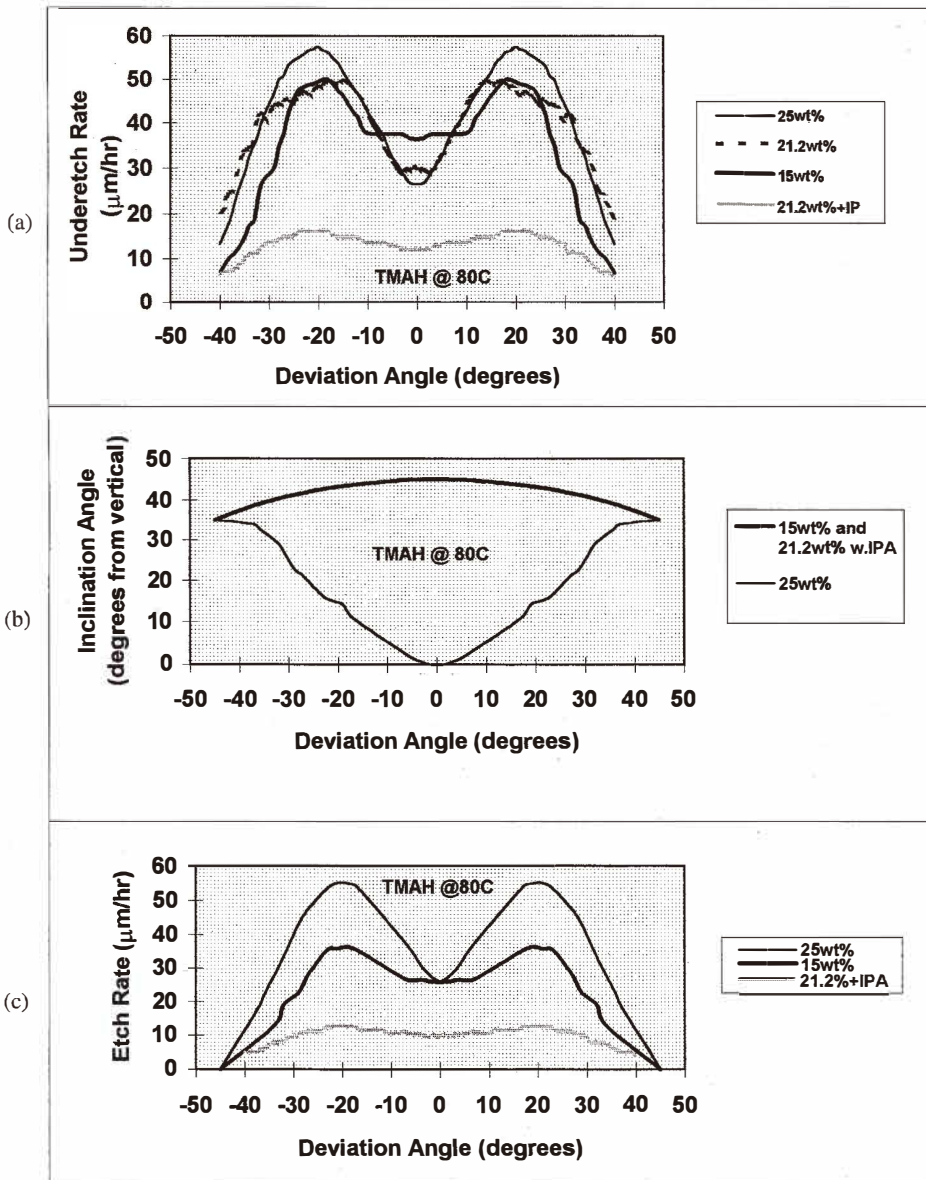


Fig. 2. (a) Under-etch rate, (b) inclined plane angle and (c) derived etch rate, versus deviation angle of oxide mask edge for lightly doped n-type Si etched in fresh TMAH at 80°C . Deviation angle is measured from the intersection of (001) and (100), which is 45° from the wafer flat. The error in the under-etch measurements and etch rates represented above is estimated to be $\pm 3 \mu\text{m}$ and $\pm 4 \mu\text{m}$, respectively (after the curves have been smoothed).

Table 1
Anisotropy of Si etched in TMAH at 80°C.

	Slowest-etch	Slow-etch	Fast-etch
25 wt%	very deep min. at {111} planes	deep min. at $\delta = 0$ in $\langle 100 \rangle$ -direction (vertical sidewalls)	high max. at $\delta \sim \pm 20^\circ$ near $\langle 522 \rangle$ -direction
21.2 wt%	very deep min. at {111} planes	min. around $\delta = 0$ (both $\langle 100 \rangle$ - and $\langle 110 \rangle$ -directions)	max. not well defined at $15^\circ \leq \delta \leq 30^\circ$
21.2 wt% w IPA	very deep min. at {111} planes	shallow min. at $\delta = 0$ in $\langle 110 \rangle$ -direction (45°-incl sidewalls)	slight max. at $\delta \sim \pm 20^\circ$ near $\langle 552 \rangle$ -direction
15 wt%	very deep min. at {111} planes	shallow min. at $\delta = 0$ in $\langle 110 \rangle$ -direction (45°-incl sidewalls)	slight max. at $\delta \sim \pm 20^\circ$ near $\langle 552 \rangle$ -direction

2.4. Comparison of under-etched planes in 25 wt% and 15 wt%

Figure 3 illustrates the different under-etched inclined planes and features at $\delta = 0$. In 15 wt% TMAH, the sidewall is at 45° to the horizontal, a {110} plane. As seen in Fig. 2(c), the etch rate of this {110} plane is about 26 $\mu\text{m/hr}$, substantially less than the 36 $\mu\text{m/hr}$ etch rate of the horizontal {100} base plane. In 25 wt% TMAH, however, the situation is quite different. The sidewall is vertical for most of its height. A small footing is present, inclined at $\sim 45^\circ$. The etch rate of the vertical {100} plane is, as expected, very close to that of the horizontal {100} base plane, about 25 $\mu\text{m/hr}$.

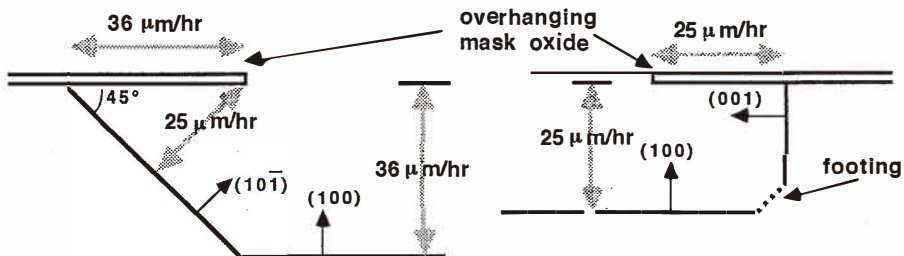


Fig. 3. Schematic of cross section of under-etched inclined planes at $\delta = 0^\circ$. At left is a 45°-inclined {110} plane, while at right is a vertical {100} plane, with a small \sim {110} footing.

The variation of the inclined plane angle with δ in TMAH 15 wt% at 80°C is very similar to the findings for 15 wt% at 50°C using a high dissolved silicon concentration reported in ref. 19. That variation has been modelled⁽¹⁹⁾ to arise from a low rate of attack of <101>-directed ledges in the silicon lattice. In other words, the under-etched inclined planes are made up mostly of intact <101> ledges for all δ . On the other hand, the formation of the vertical {100} walls, and the variation of the inclined plane in the 25 wt% case, can only occur by a rapid rate of attack of such ledges. The development in ref. 19 implies that the rate of attack of kinks must be greater than that of ledges in the 25 wt% case. In view of the above, these two cases are used to analyze the 21.2 wt% cases below.

2.5 TMAH 21.2% without IPA – An intermediate case

In TMAH 21.2 wt% without IPA, the situation is quite complicated, and can be viewed roughly as a combination or transition between the two cases described above. There are at least three regimes of deviation angle, $30^\circ \leq |\delta| \leq 45^\circ$, $15^\circ \leq |\delta| \leq 30^\circ$ and $0 \leq |\delta| \leq 15^\circ$.

Within 15° of the {111} planes ($30^\circ \leq |\delta| \leq 45^\circ$), the under-etched inclined planes have an angle of about 35° from the vertical, similar to both the 25 wt% and the 15 wt% cases. In the range $15^\circ \leq |\delta| \leq 30^\circ$, the under-etched inclined surface is so rough that it cannot be called a plane. An example of this is shown for $\delta = 18^\circ$ in Fig. 4(a). In the range of $0 \leq |\delta| \leq 15^\circ$, the under-etched surfaces are made up of two sub-planes. There is a steeper plane at the top and a shallower plane at the bottom of the under-etched surface. An example of this is shown in Fig. 4(b). The shallower plane inclination angles follow roughly the same curve as the 15 wt% case described in Fig. 2(b), and the steeper plane inclination angles follow roughly the same curve as the 25 wt% case. Figure 4(c) schematically illustrates the two planes and their proportions. The projection of the steeper plane onto the vertical is shorter than the projection of the shallower plane onto the vertical. For example, at $\delta = 0^\circ$, the vertical {100} plane extends down from the top surface to about 40% of the etch depth, while at $\delta = 10^\circ$, the top plane (about 5° from vertical), extends down from the top surface to about 25% of the etch depth. This percentage decreases monotonically as δ increases.

The above-described three regimes can be seen to loosely match the features of the under-etch curve for 21.2 wt% in Fig. 2(a). In the range $30^\circ \leq |\delta| \leq 45^\circ$, the under-etch rate is close to that of the 25 wt% case. In the range $15^\circ \leq |\delta| \leq 30^\circ$, it appears to track the 15 wt% case, and in the range $0 \leq |\delta| \leq 15^\circ$, it generally follows the 25 wt% curve. At $\delta = 0^\circ$, it may tend to approach the 15 wt% case.

2.6. The influence of IPA

The case of TMAH 21.2 wt% without IPA can be compared with the case of TMAH 21.2 wt% with IPA. At this concentration, the presence of IPA in the etchant solution reduces the under-etch rate and under-etched plane etch rate substantially, at all values of deviation angle (δ), and significantly alters the under-etched inclined planes. As shown in Fig. 2(b), with IPA, the plane inclination angles follow the 15 wt% case, consistent with a relatively low rate of attack of ledges. Since the case of 21.2% without IPA can be seen to be in transition between the 25 wt% case (a relatively higher rate of attack of ledges) and the 15 wt% case, this suggests that the presence of IPA has reduced the rate of attack of ledges. Further testing of this phenomenon is underway.

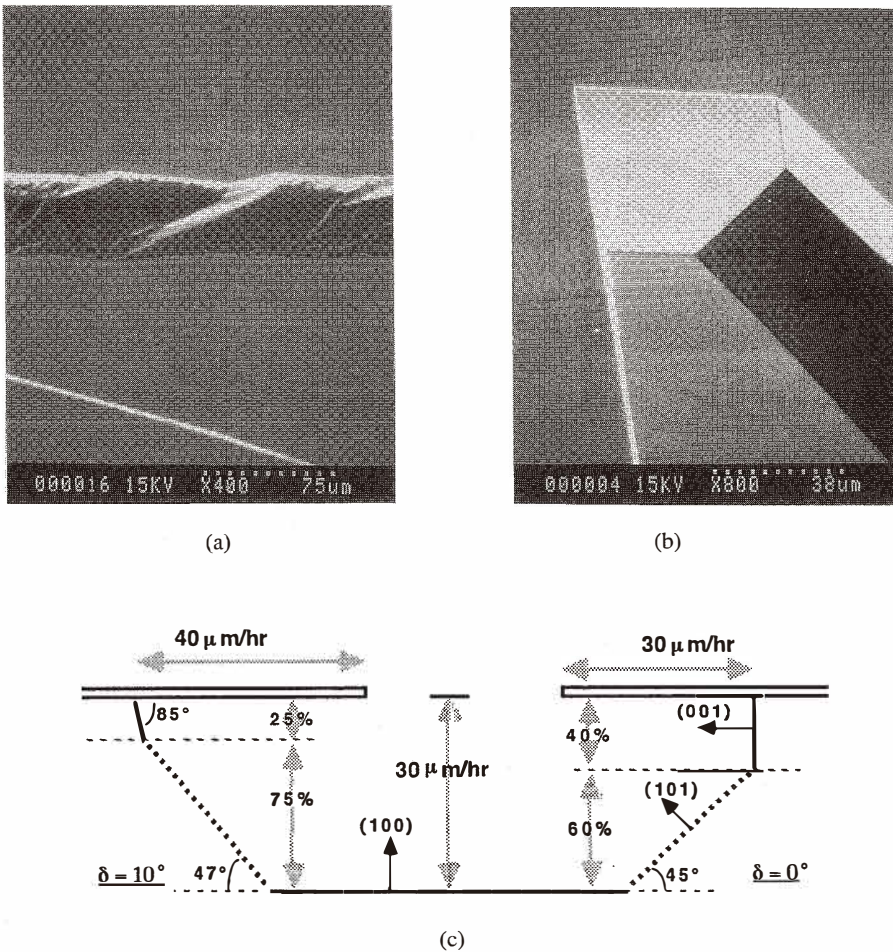


Fig. 4. Scanning electron micrographs of $\langle 100 \rangle$ wafer after under-etch experiment in TMAH 21.2%, and subsequent removal of masking oxide: (a) showing the very rough side of the etched pit of the triangle at $\delta = 27^\circ$; (b) showing (at the right side of the picture) the two-faceted side of an etch pit having $\delta \sim 0^\circ$. (c) Schematic showing the two facets of under-etched planes etched in TMAH 21.2% without IPA.

3. Conclusion

The following conclusions were noted:

- Anisotropy of silicon etched in TMAH 15 wt%–25 wt% at 80°C has been characterized by under-etch experiments, with and without IPA.

- While all cases exhibit a deep minimum in the etch rate at the {111} planes, other local minima and maxima in etch rates and under-etch rates vary substantially over the various cases studied.
- The 25 wt% and 15 wt% cases yield dramatically different under-etched inclined planes, likely stemming from relative rates of attack of ledges and kinks. These can represent two fundamental cases for the study of anisotropic etching of Si.
- The case of 21.2 wt% TMAH without IPA can be seen as a transition between the above two fundamental cases, in both the under-etch rates and in the under-etched inclined planes.

Acknowledgments

The authors would like to thank the Natural Science and Engineering Research Council of Canada (NSERC), and the Concordia-Seagram Fund for supporting this research. The support of the Can-MEMS project by the Canadian Microelectronics Corporation is also acknowledged. The authors would also like to thank Dr. N. Kapoor of Concordia University's Biology Department for the scanning electron microscopy, and Anand Pandey of Concordia University's Department of Electrical and Computer Engineering and Flavio Giacomozzi of the Istituto per la Ricerca Scientifica e Tecnologica, Italy for their technical assistance.

References

- 1 K. E. Peterson: Proceedings of the IEEE **70** (1982) 420.
- 2 H. Seidel, L. Csepregi, A. Heuberger and H. Baumgartel: J. Electrochem. Soc. **137** (1990) 3612.
- 3 D. B. Lee: J. Appl. Phys. **40** (1969) 4569.
- 4 K. E. Bean: IEEE Transactions on Electron Devices **ED25** (1978) 1185.
- 5 D. F. Weirauch: J. Appl. Phys. **46** (1975) 1478.
- 6 E. Bassous: IEEE Transactions on Electron Devices **ED25** (1978) 1178.
- 7 D. L. Kendall: Ann. Rev. of Mater. Sci. **9** (1979) 373.
- 8 J. B. Price: Semiconductor Silicon, The Electrochemical Society Softbound Symposium Series, (Princeton, NJ, 1973) 339.
- 9 M. Elwenspoek: J. Electrochem. Soc. **140** (1993) 2075.
- 10 M. Elwenspoek, U. Lindberg, H. Kok and L. Smith: IEEE Workshop on Micro-Electro Mechanical Systems (MEMS-94), Oiso, Japan, (1994) 223.
- 11 D. L. Kendall: J. Vac. Sci. Technol. A **8** (1990) 3598.
- 12 U. Schnakenberg, W. Benecke and P. Lange: The 6th International Conference on Solid-State Sensors and Actuators, Tech. Digest, (Transducers '91) San Francisco, CA, USA, June 24–28, 1991 (1991) 815.
- 13 O. Tabata, R. Asahi, H. Funabashi, K. Shimaoka and S. Sugiyama: Sensors and Actuators A **34** (1992) 51.
- 14 A. Merlos, M. C. Acero, M. H. Bao, J. Bausells and J. Esteve: J. Micromech. Microeng. **2** (1992) 181.
- 15 A. Merlos, M. Acero, M. H. Bao, J. Bausells and J. Esteve: Sensors and Actuators A **37–38** (1993) 737.

- 16 E. Steinsland, M. Nese, A. Hanneborg, R. W. Bernstein, H. Sandmo and G. Kittilsland: The 8th International Conference on Solid-State Sensors and Actuators, and Eurosensors IX, Stockholm, Sweden, June 25–29, 1995 (1995) 190.
- 17 S. Naseh: Master of Applied Science Thesis, Concordia University, September 1995, Chapters 4,5.
- 18 S. Naseh, L. M. Landsberger, M. Paranjape and M. Kahrizi: *Can. J. Phys. (Suppl.)* **74** (1996) S79.
- 19 L. M. Landsberger, S. Naseh, M. Kahrizi and M. Paranjape: *IEEE-J. Microelectromech. Sys.* **5** (1996) 106.
- 20 S. C. Chang and D. B. Hicks: *IEEE Solid-State Sensors and Actuators Workshop*, Hilton Head Island, USA (1988) 102.
- 21 L. Offereins, K. Kuhl and H. Sandmaier: *Sensors and Actuators A* **25–27** (1991) 9.
- 22 K. P. Wu and W. H. Ko: *Sensors and Actuators* **18** (1989) 207.
- 23 R. Dizon, H. Han and M. L. Reed: *IEEE Workshop on Micro-Electro Mechanical Systems (MEMS-93)*, Florida, USA (1993) 48.
- 24 C. Strandman, L. Rosengren and Y. Backlund: *IEEE Workshop on Micro-Electro Mechanical Systems (MEMS-95)*, Amsterdam, The Netherlands (1995) 244.
- 25 W. S. Choi and J. G. Smits: *IEEE-J. Microelectromech. Sys.* **2** (1993) 82.